Covalent coupling regulated thermal conductivity of Poly(vinyl alcohol)/boron nitride composite film based on silane molecular structure

Hua Cheng [‡ a, b, c], *Kai Zhao* [‡d], *Yi Gong* [*a], *Xiao Wang* [e], *Rui Wang* [a, b], *Fengyu Wang* [a], *Rui Hu* [a], *Fangkuo Wang* [c], *Xian Zhang* [a], *Jianying He* [f], *Xingyou Tian* [*a]

[a] Key Laboratory of Photovolatic and Energy Conservation Materials, Institute of Applied Technology, Hefei Institutes of Physical Science, Chinese Academy of Sciences, Hefei 230031, People's Republic of China

[b] University of Science and Technology of China, Hefei 230026, People's Republic of China

[c] Department of Chemistry and Chemical Engineering, Hefei Normal University, Hefei 230061, People's Republic of China

[d] Department of Engineering, Aarhus University, 8000 Aarhus, Denmark

[e] Reservoir Engineering Research Institute, Palo Alto, California 94301, United States

[f] Department of Structural Engineering, Faculty of Engineering, Norwegian University of Science and Technology (NTNU), 7491 Trondheim, Norway

*E-mail: yigong@rntek.cas.cn (Y. Gong), xytian@issp.ac.cn (X. Tian)

Abstract. Creating covalent bonds between inorganic fillers and polymer matrix is an effective method to enhance the thermal conductivity (TC) of composite materials, while the detailed mechanism is still not clear. By introducing different silane coupling agents (SCAs) bonding poly(vinyl alcohol) (PVA) and functionalized boron nitride (fBN), intrinsic relationship between molecular structure of silane crosslinkers and TC of PVA-fBN composite has been systematically investigated. The results show that the SCAs molecules with short side chain, *i.e.* vinyl triethoxysilane (VTES) and tetraethyl orthosilicate (TEOS), increase the TC of composite polymer, with maximum value of 1.636 W/m·K, which is 337.3% of that of PVA/fBN. In contrast, 3-glycidoxypropyltrimethoxy silane (GPTMS) with long side chain decreases the TC to 54.4% of that of PVA-fBN. The number of hydrolyzable Si-O-R of SCAs molecules affects the TC of PVA-fBN composite through controlling the self-condensation degree of SCAs. Integrated with atomistic simulations, these findings provide new insights for the design of polymer-based thermal management materials.

Keywords. thermal conductivity, covalent coupling, molecular structure, silane coupling agents, poly(vinyl alcohol), functionalized boron nitride

1. Introduction

Miniaturization and high power density of nano/micro electronic systems cause significant heat accumulation, limiting the efficiency and lifespan of the devices [1-3]. As common electronic packaging material, polymers exhibit a low intrinsic thermal conductivity, usually in an order of 0.1 W/m·K) [4]. Introduction of fillers with high thermal conductivity (TC), such as carbon materials [5, 6], ceramic materials [7-10] and metallic particles [4, 11], has been proven as an effective and scalable method to improve the TC of polymer matrix, thus enhancing heat dissipation performance of electronic devices. However, the interface between fillers and polymer matrix is believed to be the bottleneck of the heat transfer in the composite material [12, 13]. Phonon, the heat carrier of polymer system, could be easily scattered by the interface, which limits the overall TC of the composite [14-22]. Tremendous efforts have been done for decreasing the interfacial thermal resistance between the filler and polymer matrix through either non-covalent bonding or covalent bonding. Typical non-covalent bonding includes the weak molecular interaction such as π-π stacking, hydrogen bonding electrostatic adsorption and so on. *Via* creating electrostatic adsorption between positively charged polystyrene (PS) microspheres and negatively charged boron nitride nanosheets (BNNS), Wang *et al.* reported that the TC for PS/BNNS composites could reach 8.0 W/m·K at 13.4 vol% BN loading [19]. Hydrogen bond enhanced interfacial adhesion between BNNS fillers and poly(vinyl alcohol) (PVA) matrix lifted TC of the composite in parallel direction to 18.63 W/m·K by electrospinning and hot-pressing technology [23]. Our previous study revealed that the π−π stacking and van der Waals interactions between BN and styrene could be employed to construct thermally conductive polymer composite based on Pickering emulsion template [18]. By utilizing the noncovalent functionalized BNNS and PVA, Zeng *et al.* obtained artificial nacre-like papers with excellent

tensile strength (125.2 MPa) and high TC (6.9 W/m·K) [7]. Non-covalent bonding between the fillers and polymer interface weakens the phonon scattering and bridges their vibrational mismatch [16], thus decreasing the interfacial thermal resistance under relative mild fabrication conditions.

Compared with non-covalent interaction, covalent bonding offers permanent attachments between fillers and polymers, effectively constraining the corresponding scattering of phonons [4]. Furthermore, covalent functionalization of filler is beneficial to the filler dispersion in polymer matrix [14]. Abundant researches have been dedicated to filler surface modification for creating covalent bonds and thus decreasing thermal interfacial resistance. Wang *et al.* found that butyl group showed excellent effectiveness among the various functional groups on reducing the interfacial thermal resistance of functionalized graphene system [20]. 1,4-butanediol diglycidyl ether (BDGE) was used as the covalent cross-linker by Ding *et al.* to fabricate dual-cross-linked thermo-responsive polymeric composites, reaching maximum 10 °C reduction in work temperature [8]. By grafting γ-methacryloxypropyl trimethoxy silane (KH570) on BN plates in the nature rubber, 4 times improvement TC was achieved [21].

Although covalent bonding shows effectiveness on decreasing interfacial thermal resistance in many scenarios, the introduced molecules wrapped on the surrounding of fillers can possibly act as thermal barriers. For instance, a "trade-off" effect related to the quantity of silane coupling agents (SCAs) has been reported that low concentration SCAs increased the TC of the composites while high concentration decreased the value [24]. Up to date, the importance of the dosage of SCAs was widely emphasized in the literatures [25, 26]. In order to clarify the effect of SCAs on the TC of the composite, in present study, hexagonal boron nitride filler and PVA matrix were crosslinked with three different SCAs. The revealed intrinsic relationships between

TC of the composite and molecular structure of SCAs provide a new perspective to understand the covalent bonding regulated TC of the polymer/filler system. This study will guide thermal management material design on the molecular level, further supporting the development of advanced electronics.

2. Materials and experimental methods

2.1.Materials

Hexagonal BN (h-BN, CAS no.: 10043-11-5; purity> 98%, diameter = 2–3μm) was supplied by Dandong Rijin Science and Technology Co., Ltd. Poly (vinyl alcohol) (PVA, CAS no.: 9002-89-5; purity> 98%, polymerization degree = 1700 and alcoholysis degree= 99%) was purchased from Aladdin Reagent Co., Ltd. Tetraethyl orthosilicate (TEOS, CAS no.: 78-10-4; purity> 99.99%), vinyl triethoxysilane (VTES, CAS no.: 78-08-0; purity> 97%) and 3-glycidoxypropyltrimethoxy silane (GPTMS, CAS no: 2530-83-8; purity> 98%) were purchased from Aladdin Reagent Co., Ltd. Isopropanol (CAS no.: 67-63-0; AR) and hydrochloric acid (CAS no: 7647-01-0; purity>97%) was purchased from Sinopharm Chemical reagent Co., Ltd. All reagents were used as received. Deionized water was fabricated from Milli-Q water purification system.

2.2.Functionalization of h-BN

As suggested in literatures [27, 28], functionalization of h-BN was carried out as following procedures. First, 1 g pristine h-BN powders were dispersed into a 100 mL mixture of isopropanol and deionized water (4:1 V/V) with the aid of an ultrasonic bath (600 W, 40 KHz) for 7 hours. The obtained dispersion was then standing for 2 hours to remove “non-cutting” BN sheets. After centrifugation at 9000 rpm for 15 min, functionalized BN was collected (labelled as fBN) and dried in the vacuum oven at 60℃more than 12 hours.

2.3.Preparation of PVA-SCA-fBN composites

PVA was dissolved in deionized water by stirring at 95 ºC for 4 hours to obtain 4 wt% PVA solution. 0.4 g fBN powders were dispersed into 20 ml PVA solution by 30 min sonication, then various amounts of SCAs (0.00175 mol, 0.0035 mol, and 0.007 mol) were added into the abovementioned mixtures, respectively. pH of the mixtures was adjusted to 3.0 by adding 1 mol HCl, and chemical reaction was maintained 24 hours at 35 ℃ under 750 rpm stirring. The obtained mixtures were poured into organic glass plates and dried at room temperature for 3 days to obtain composite films. The composite films were dried in the vacuum oven at 60 ℃ for 12 hours before further characterization.

2.4.Characterization

Fourier-transform infrared spectroscopy (FT-IR, Spectrum Two, Pekin Elmer) as well as X-ray photoelectron spectroscopy (XPS, ESCALAB 250Xi, Thermo Fisher) were used to analyze the chemical composition of the samples. The morphology of fBN and cross-section of composite film were characterized by scanning electron microscopy (SEM, Sirion-200 FEI, America). Energy dispersive spectroscopy (EDS) detector in SEM was used to detect the element distribution of samples. Philips X'Pert Pro MPD X-ray diffractometer with Cu K-α radiation (λ = 0.154 nm, 40 kV, 40 mA) was utilized to investigate the structure of fBN and the composites. To test the mechanical properties of the composites, dynamic mechanical analysis (DMA Q800) was used for tensile testing at room temperature and the composites were cut into 5×30 mm strips. Digital vernier caliper was utilized to measure the thickness and width of each strip. The measurement was performed at tensile rate of 5 mm/min. Hot Disk instrument (TPS 2200, AB Corporation, Sweden) in anisotropy mode was adopted to measure the thermal conductivity of the composites. Each measurement was repeated five times. Infrared camera (FOTRIC 220s,

China) was used to record the temperature distribution evolution of the composites on a programmable heating device heated from 22 to 58°C. Composite films with mean diameter of 20 mm and mean thickness of 0.12 mm were integrated into a self-made Light-emitting-diode (LED) lamp (3 watts) device as a substrate. After 2 mins working of LED lamp, surface temperature of composite film was recorded by infrared camera.

2.5.Atomistic simulation

To further illustrate the effect of distinct SCAs on the thermal performance of the composites, long-time atomistic simulations were carried out to calculate the TC. The simulations were performed using the open source molecular dynamics (MD) code LAMMPS [29]. Sandwich-like cross-linked interface models (as shown in Fig. S1 in the Supporting Information) were built to model the experimental setting-up. Interatomic forces of the fBN layer were computed using the three-body Tersoff potential [30], while the atomic interactions of polymer molecules were described by the Consistent Valence Force-Field (CVFF) [31]. Periodic boundary condition was applied along the x- and z-directions, and the TC was computed in the y-direction, along which the boundary was set as shrink-wrapped. The timestep was set as 0.5 fs for all simulations. The fundamental structural unit was energetically minimized, and replicated as a 5×2×1 system in the Cartesian coordinate system. The sandwich-like configuration was then equilibrated to the minimum energy state using conjugate gradient algorithm, and relaxed at 500 K using a Langevin thermostat. The atomic position and velocity were initially updated under NVE ensemble, with a maximum distance 0.05 Å per timestep. Then, the equation of motion was integrated under NPT ensemble sequentially with different temperatures, i.e. (1) 500 K; (2) 500 −> 100 K; (3) 100 −> 300 K; and (4) 300 K to relax any high energy configurations. The system was then relaxed under NVT ensemble for 250 ps at 300 K before calculating TC using the

Green-Kubo method, which relates the ensemble average of the auto-correlation of the heat flux $\mathbf{J}$ to the TC,

$$\kappa = \frac{V}{3k_B T^2}\int_0^\infty \langle \mathbf{J}(0)\cdot\mathbf{J}(t)\rangle \mathrm{d}t \qquad \text{equation 1}$$

where V and T are the system volume and temperature, and k_B is the Boltzmann constant.

3. Results and discussion

3.1. BN functionalization

Hydroxylation of BN platelets was carried out in order to create potential crosslinking sites on the surface. By sonication-assistant exfoliation, B-N bonds of pristine BN platelets near defect sites were opened by oxygen atom, so that pendant hydroxyl groups could be formed [27]. Characteristic peaks in FT-IR spectra (Fig. 1a) located at 1373 cm^{-1} and 802 cm^{-1} are ascribed to B-N stretching vibration while that of 3434 cm^{-1} is ascribed to the -OH stretching vibration [32, 33]. The intensity of -OH stretching for functionalized boron nitride (fBN) is much stronger compared to pristine BN, revealing that the number of -OH groups is increased after hydroxylation. Multipeak Gaussian method was utilized to fit the high-resolution XPS spectra of B 1s and N 1s. As shown in Fig. 1b, the B 1s spectrum is split into two peaks locating at 191.3 and 190.6 eV, which are attributed to the B−O and B−N bonds, respectively [18]. It indicates that the -OH groups are bonded to B atoms of fBN, agreeing well with the results of Lin's work [15]. The XRD pattern (Fig. 1c) suggests a well-preserved structural integrity of fBN after hydroxylation [3]. fBN exhibited thin sheets-like morphology in the SEM image (Fig. 1d) with lateral sizes ranging from 0.37-1.28 μm (average lateral size 0.74 μm), smaller than that of pristine BN (2–3μm) before hydroxylation due to the cutting effect. The TEM image (Fig. 1e) also confirms the lattice fringes of fBN at a spacing of 0.25 nm in Fig. 1f corresponding to the (002) crystal plane [34]. Fast Fourier transform image shows (inset of Fig. 1f) a clear six-fold

symmetry of fBN [35] associated with the (002) plane [3] in XRD pattern (Fig. 1c), which also indicates the hexagonal lattice structure of BN is retained after hydroxylation.

3.2. SCAs coupling between PVA and fBN

PVA and fBN were chemically coupled by SCAs in the resulting composite films, the corresponding molecular structures were verified by FT-IR, XPS and XRD spectra. After added into the mixture of PVA and fBN suspension, SCAs were hydrolysed to silanol in acid environment. It is confirmed by that only characteristic peak of alkyl group at 2945 cm^{-1} is observed in FT-IR spectra of composites (Fig. 2a), while the absorption bands locating at 2840 cm^{-1} and 2980 cm^{-1} are missing resulted from the stretching of C-H bonds in methoxy group and ethoxy group of SCAs, respectively [36,37]. Then the hydrolysed SCAs have three possible reactions including: self-condensation, PVA crosslinking and fBN bonding.

Self-condensation. Silica was formed due to the self-condensation of hydrolyzed SCAs, which is indicated by that the characteristic symmetric stretching of Si-O-Si centered at 849 cm^{-1} [38] in Fig. 2b. The degree of self-condensation is determined by the molecular structure of SCAs. Si-OH stretching vibration at 917 cm^{-1} [39] observed in PVA-VTES-fBN and PVA-GPTMS-fBN implies inadequate self-condensation of VTES and GPTMS. No such signal is found in PVA-TEOS-fBN, suggesting stronger self-condensation of TEOS compared to the other two SCAs. Cluster analysis in MD simulation shows the same trend. In the equilibrated system of identical number of SCAs molecules, the TEOS condensates into 7 clusters, VTES forms 3 clusters, while the GPTMS molecules distribute homogeneously at room temperature (Fig. S2 in the Supporting Information).

PVA crosslinking. SCAs showed different reactive site and reactivity during the PVA crosslinking reaction. Si-O-C asymmetric stretching vibration peak located at 965 cm^{-1} [40] is

observed in PVA-TEOS-fBN and PVA-VTES-fBN system (Fig. 2b). However, no such peak can be found in PVA-GPTMS-fBN, suggesting insufficient reaction of hydroxyl groups in GPTMS with PVA. The vanished characteristic peak of epoxy groups centered at 908 cm^{-1} suggests that epoxy rings of GPTMS were opened by reacting with hydroxyl groups of PVA in acid condition [41, 42]. The newly-formed C-O-C bond could be verified by the peak at 1200 cm^{-1} (Fig. 2b) [41]. Reactivity of SCAs towards PVA was quantitatively analyzed by the C-OH content of PVA, which were estimated by high-resolution C 1s elemental scans of the composite films in Fig. 2c-2f according to the literatures [43, 44]. The binding energy of the C–C and C–H bonding from PVA backbone are assigned at 284.8 eV and other functional groups are assigned as followings: C-OH (286.4 eV), C-O-C (287.5 eV) ,C=O (288.4 eV), and O-C=O (289.3 eV) [43-47]. The estimated C-OH content is 32.46% (Fig. 2c) in pure PVA, and decreases to 20.84% (Fig. 2d), 10.89% (Fig. 2e) and 27.23 % (Fig. 2f) after reaction with TEOS, VTES and GPTMS, respectively. TEOS exhibited weaker reactivity to PVA compared to VTES, because its strong self-condensation decreased the amount of active Si-OH. GPTMS showed the least reactivity to PVA. The reaction between SCAs and hydroxyl groups in PVA in the crystalline domains also led to the expansion of the amorphous region. $2\theta = 20°$ in XRD pattern (Fig. 2g) is attributed to the mixture of (101) and (200) crystallographic planes of PVA [48]. The intensity of peak $2\theta = 20°$ of PVA-fBN is lower than pure PVA due to the formed hydrogen bonds between PVA and fBN. The peak intensity at $2\theta = 20°$ in composite films with VTES, TEOS and GPTMS increases gradually, indicating a decreasing crosslinking degree, agreeing well with the FT-IR results.

fBN bonding. When SCAs coupled PVA/fBN composites, the bonding between silane and fBN would affect the periodic structure of nanosheets [49, 50], which was confirmed by the decreasing intensity of the peak $2\theta = 26.7°$ ((002) face of BN) in XRD pattern for GPTMS,

TEOS, VTES (Fig. 2g). The intensity of peak at 2θ = 26.7° would recover when the amount of added SCAs decreased (Fig. 2h), also supporting the above argument. The severe deformation of BN layers observed in MD simulation (see Fig. 2i-2k) also agrees well with that SCAs bonding would distort BN lattice structure. The possible reactions are illustrated in Fig. 3 and detailed chemical reaction could be found in the Supporting Information.

3.3. Microstructure of the composites

PVA-SCA-fBN composite films were fractured to create surfaces for microstructure investigating by SEM observation. BN platelets could be pulled-out during the fracture, leaving cavities which were used as an indicator for evaluating the bonding effect between the filler and polymer matrix [24, 51]. Cavities, labelled by yellow circle in Fig. 4a, could be found at the fracture surface of PVA-fBN composite film (without SCAs coupling), indicating weak connection between polymer and filler. After addition of TEOS, BN platelets are surrounded by PVA matrix in Fig. 4b. Specifically, the covalent bonds derived from TEOS could bridge the fillers and matrix, and the enhanced interfacial adhesion decreased the amount of cavities. No obvious cavities are found in VTES-crosslinked PVA matrix where BN platelets are dispersed homogeneously (Fig. 4c), suggesting a strong interfacial bonding. However, obvious cavities are found in Fig. 4d in the system of GPTMS, ascribed to the poor interfacial interaction between fBN and the polymer matrix. Furthermore, Fig. 4e and Fig. 4f show N element from fBN is surrounded by Si element in EDS maps of PVA-TEOS-fBN and PVA-VES-fBN, implying good compatibility between BN and SCAs. However, voids between N and Si elements could be observed in PVA-GPTMS-fBN (Fig. 4g), due to the low reactivity of GPTMS towards Si-OH and fBN. The SCAs bonding effect between the filler and matrix also affects the mechanical properties of the composite film, which are discussed in Supporting Information.

3.4. Thermal conductivity of composites

SCA molecular structure showed dramatic influence on TC of the composite films. TC of PVA-fBN (without SCAs) was 0.485 W/m·K, which changed to 0.387, 1.005 and 0.675 W/m·K after addition of 0.00175 mol TEOS, VTES and GPTMS, respectively. TC of the composite films increased with the increasing SCAs loading in the TEOS and VTES system, while the opposite trend was found in the case of GPTMS. Further increasing SCAs content from 0.0035 mol to 0.007 mol, TC of PVA-VTES-fBN climbed to 1.241 and 1.636W/m·K, respectively (Fig. 5a). TEOS showed similar trend with VTES during this process, however, increasing GPTMS content decreased the TC from 0.675 to 0.264 W/m·K. Number of hydrolyzable Si-O-R and length of side chains in SCAs molecule are demonstrated to be the critical parameters controlling the TC of the composite film.

Number of hydrolyzable Si-O-R. As discussed above, Si-O-R of SCAs would hydrolyze to Si-OH, which either bonds PVA/fBN or forms silica by self-condensation. TEOS and VTES could form Si-O-C (with PVA) and Si-O-B (with fBN) in composite film, supporting firm covalent bonding between PVA and fBN. Compared with non-covalent bonding, the formed covalent bond could promote phonon (heat-carrier) transfer at material interface[52,53]. So the enhanced interfacial bonding between polymer and fillers dramatically decreases the interfacial thermal resistance and elevates the TC of the composite film. There is vinyl group (containing C=C bond) on silicon atom of VTES molecule. It makes VTES has one less hydrolyzable Si-O-R compared with TEOS, thus decreasing the possibility of VTES self-condensation. As a result, more available VTES molecules could provide polymer/filler bonding thus showing better TC improvement compared to TEOS. It suggests there was a competition effect between polymer/filler bonding and self-condensation of SCAs, thus SCAs with 4 hydrolyzable Si-O-R

showed declined performance on polymer/filler bonding compared to that of 3 Si-O-R. Number of Si-O-R also affects the sensitivity of TC to the SCAs loading. As increasing SCAs amount from 0.0035 mol to 0.007 mol, sample with TEOS showed negligible improvement on TC compared to VTES. It may be ascribed to that Si-OH in TEOS is preferable to proceed self-condensation compared to PVA/fBN bond in high concentration.

Length of side chain. GPTMS shows a longer 3-glycidoxypropyl side chain (8.170 Å) compared with that of VTES (4.989 Å) as shown in Fig. 3. Low concentration (0.00175 mol) of GPTMS slightly increased the TC of the composite due to the brought covalent bonding. However, unlike VTES, further increasing amount of GPTMS led to the decreasing TC. GPTMS covalently bonds PVA/fBN from the epoxy ring end (Fig. 3), which brings the long side chain into thermal conductive pathway. The decreasing TC of the composite film implies that the long side chain could decline the thermal conduction. Since that GPTMS bonds the PVA and fBN via longer side chains (see Fig. 3), which is different from the other two SCAs (*via* Si-O-R), MD simulation were used to verify our speculation where GPTMS was set to bond PVA and fBN with B-O-R. The interfacial TC of SCAs-coupled fBN/PVA from MD calculations are 958.9, 1252.8 and 43.2 W/m·K for TEOS-, VTES-, and GPTMS-crosslinked system, indicating that, even not included in the thermal conductive pathway, the length of side chain has a negative effect on the TC of PVA/fBN. It could be caused by that the long side chain increases the disorder of the vicinal molecular structure, which limits the phonon transferring. The calculation of radial distribution function (RDF in Fig. 5b) further demonstrates that the effect of SCAs on TC is attributed to the variation of the first- and second-nearest atomic population, which could originate from the steric hindrance of the long side chain. These results follow the same trend found in the experiments, although the absolute values are much larger since the present

computational models (shown in Fig. S1) was performed in limited scale where structural defects, such as voids and boundaries in practical experiments could not be considered.

3.5. Heat dissipation performance of composite films

As shown in Fig. 6, thermal imaging tests were carried out to investigate the heat conduction performance of the composites in the practical working conditions. The temperature of film top-surface was acquired by the IR camera as a function of time while the downside was heated simultaneously. The heat conduction abilities of the composite films agree well with the trend of TC. As depicted in Fig. 6a, the surface temperature of PVA-VTES-fBN responds faster to the heating compared to other samples. Infrared thermal images of the temperature evolution (Fig. 6b) corresponding to the composites during heating is also consistent with the results of TC measurements, indicating that SCAs essentially determine the heat dissipation performance of PVA-SCAs-fBN system. The composite films were integrated into LED device as a substrate to evaluate the heat dissipation performance in a model electronics, as illustrated in Fig. 6c. Temperatures of LED lamp with PVA-VTES-fBN, PVA-TEOS-fBN and PVA-GPTMS-fBN reached to 23.1 ℃, 23.3 ℃ and 23.8 ℃ in 2 mins, respectively (Fig. 6d). Due to the low TC, LED with PVA-GPTMS-fBN substrate showed rapidly increased temperature in 1 min. In contrast, LED with PVA-VTES-fBN substrate exhibited slow increasing trend of temperature, and eventually led to 0.7 ℃ reduction on the hot spot temperature compared with PVA-GPTMS-fBN substrate.

4. Conclusions

In summary, the effect of SCAs molecules on TC of PVA/fBN composites was investigated. SCAs were confirmed to be able to provide covalent bonding between PVA/fBN. Number of hydrolyzable Si-O-R and length of side chains in SCAs molecules are proposed to be the critical

parameters controlling the TC of the composite film. Owing to the desired molecular structure, VTES improved TC of PVA/fBN composite film to 1.636 W/m·K, best among other investigated SCAs. SCAs structure induced temperature reduction on LED device with composite film substrate is demonstrated. The mechanism of SCAs regulated TC of the PVA/fBN system was proposed based on the experiment and atomistic simulations, giving scientific guidance to polymer-based thermal management material design.

Acknowledgment

The authors gratefully acknowledge the financial supports from the National Key Research and Development Program of China (2017YFB0406200); Science and Technology Service Network Program of CAS (KFJSTS-ZDTP-069); Youth Innovation Promotion Association CAS (Grant No. 2020446); Anhui Provincial Natural Science Foundation (1908085QB64 and 1808085QE160); CASHIPS (Hefei Institutes of Physical Science, CAS) Director's Fund (YZJJ2019QN23); Young Teachers Special Project of Hefei Normal University (2017QN17); Excellent Talent Foundation of Education Department of Anhui Province (gxyq2018055); The Natural Science Foundation of the Education Department of Anhui Province (KJ2019A0731); Key Lab of Photovoltaic and Energy Conservation Materials, CAS; and Anhui Province Key Laboratory of Environment-friendly Polymer Materials. The Research Council of Norway is acknowledged for the grant to project no. 251068 Engineering Metal−Polymer Interface for Enhanced Heat Transfer.

Supporting Information Available

The following files are available free of charge. Computational models (Fig S1), self-condensation of SCAs (Fig S2), mechanical properties of the composites (Fig S3, Table S1)

chemical reactions describing the coupling effect of SCAs to the PVA and fBN(Fig S4-S6), thermal conductivity comparison of polymer composites containing fillers proceeded by different functionalization treatments (Table S2) could be found in Supporting Information (PDF).

Author Contributions

‡ Contributed equally to this work.

Notes

The authors declare no competing financial interest.

References

[1] Cui ZH, Oyer AJ, Glover AJ, Schniepp HC, Adamson DH. Large Scale Thermal Exfoliation and Functionalization of Boron Nitride. Small 2014;10(12):2352-2355.

[2] Fu L, Wang T, Yu J, Dai W, Sun H, Liu Z, et al. An ultrathin high-performance heat spreader fabricated with hydroxylated boron nitride nanosheets. 2D Mater 2017;4(2):1-7.

[3] Shao L, Shi L, Li X, Song N, Ding P. Synergistic effect of BN and graphene nanosheets in 3D framework on the enhancement of thermal conductive properties of polymeric composites. Compos Sci Technol 2016;135:83-91.

[4] Chen H, Ginzburg VV, Yang J, Yang Y, Liu W, Huang Y, et al. Thermal conductivity of polymer-based composites: Fundamentals and applications. Prog Polym Sci 2016;59:41-85.

[5] Yu A, Ramesh P, Sun X, Bekyarova E, Itkis ME, Haddon RC. Enhanced Thermal Conductivity in a Hybrid Graphite Nanoplatelet – Carbon Nanotube Filler for Epoxy Composites. Adv Mater 2008;20(24):4740-4744.

[6] Chen W, Li S, Chen C, Yan L. Self-assembly and embedding of nanoparticles by in situ

reduced graphene for preparation of a 3D graphene/nanoparticle aerogel. Adv Mater 2011;23(47):5679-5683.

[7] Zeng X, Ye L, Yu S, Li H, Sun R, Xu J, et al. Artificial nacre-like papers based on noncovalent functionalized boron nitride nanosheets with excellent mechanical and thermally conductive properties. Nanoscale 2015;7(15):6774-6781.

[8] Jiang F, Cui S, Rungnim C, Song N, Shi L, Ding P. Control of a Dual-Cross-Linked Boron Nitride Framework and the Optimized Design of the Thermal Conductive Network for Its Thermoresponsive Polymeric Composites. Chem Mat 2019;31(18):7686-7695.

[9] Yin CG, Ma Y, Liu ZJ, Fan JC, Shi PH, Xu QJ, et al. Multifunctional boron nitride nanosheet/polymer composite nanofiber membranes. Polymer 2019;162:100-107.

[10] Guerra V, Wan CY, McNally T. Thermal conductivity of 2D nano-structured boron nitride (BN) and its composites with polymers. Prog Mater Sci 2019;100:170-186.

[11] Misiura AI, Mamunya YP, Kulish MP. Metal-Filled Epoxy Composites: Mechanical Properties and Electrical/Thermal Conductivity. J Macromol Sci B 2019; 59:121-136.

[12] Burger N, Laachachi A, Ferriol M, Lutz M, Toniazzo V, Ruch D. Review of thermal conductivity in composites: Mechanisms, parameters and theory. Prog Polym Sci 2016;61:1-28.

[13] Song J, Zhang Y. Effect of an interface layer on thermal conductivity of polymer composites studied by the design of double-layered and triple-layered composites. Int J Heat Mass Transf 2019;141:1049-1055.

[14] Hong J, Lee J, Hong CK, Shim SE. Effect of dispersion state of carbon nanotube on the thermal conductivity of poly(dimethyl siloxane) composites. Curr Appl Phys 2010;10(1):359-363.

[15] Jing L, Li H, Tay RY, Sun B, Tsang SH, Cometto O, et al. Biocompatible Hydroxylated

Boron Nitride Nanosheets/Poly(vinyl alcohol) Interpenetrating Hydrogels with Enhanced Mechanical and Thermal Responses. ACS Nano 2017;11(4):3742-3751.

[16] Lin S, Buehler MJ. The effect of non-covalent functionalization on the thermal conductance of graphene/organic interfaces. Nanotechnology 2013;24(16):165702-165708.

[17] Pan C, Kou K, Jia Q, Zhang Y, Wu G, Ji T. Improved thermal conductivity and dielectric properties of hBN/PTFE composites via surface treatment by silane coupling agent. Compos Pt B-Eng 2017;111:83-90.

[18] Wang R, Cheng H, Gong Y, Wang F, Ding X, Hu R, et al. Highly Thermally Conductive Polymer Composite Originated from Assembly of Boron Nitride at an Oil-Water Interface. ACS Appl Mater Interfaces 2019;11(45):42818-42826.

[19] Wang X, Wu P. Preparation of Highly Thermally Conductive Polymer Composite at Low Filler Content via a Self-Assembly Process between Polystyrene Microspheres and Boron Nitride Nanosheets. ACS Appl Mater Interfaces 2017;9(23):19934-19944.

[20] Wang Y, Zhan HF, Xiang Y, Yang C, Wang CM, Zhang YY. Effect of Covalent Functionalization on Thermal Transport across Graphene–Polymer Interfaces. J Phys Chem C 2015;119(22):12731-12738.

[21] Yang D, Ni YF, Kong XX, Gao DH, Wang Y, Hu TT, et al. Mussel-inspired modification of boron nitride for natural rubber composites with high thermal conductivity and low dielectric constant. Compos Sci Technol 2019;177:18-25.

[22] Zhang J, Li C, Yu C, Wang X, Li Q, Lu H, et al. Large improvement of thermal transport and mechanical performance of polyvinyl alcohol composites based on interface enhanced by SiO2 nanoparticle-modified-hexagonal boron nitride. Compos Sci Technol 2019;169:167-175.

[23] Yang X, Guo Y, Han Y, Li Y, Ma T, Chen M, et al. Significant improvement of thermal

conductivities for BNNS/PVA composite films via electrospinning followed by hot-pressing technology. Compos Pt B-Eng 2019;175,1-7.

[24] Zhou W. Effect of coupling agents on the thermal conductivity of aluminum particle/epoxy resin composites. J Mater Sci 2011;46(11):3883-3889.

[25] Hong JP, Yoon SW, Hwang TS, Lee YK, Won SH, Nam JD. Interphase control of boron nitride/epoxy composites for high thermal conductivity. Korea-Aust Rheol J 2010;22(4): 259-264.

[26] Lee B, Dai G. Influence of interfacial modification on the thermal conductivity of polymer composites. J Mater Sci 2009;44(18):4848-4855.

[27] Lin Y, Williams TV, Xu TB, Cao W, Elsayed-Ali HE, Connell JW. Aqueous Dispersions of Few-Layered and Monolayered Hexagonal Boron Nitride Nanosheets from Sonication-Assisted Hydrolysis: Critical Role of Water. J Phys Chem C 2011;115(6):2679-2685.

[28] Chen J, Huang X, Zhu Y, Jiang P. Cellulose Nanofiber Supported 3D Interconnected BN Nanosheets for Epoxy Nanocomposites with Ultrahigh Thermal Management Capability. Adv Funct Mater 2017;27(5):1604754.

[29] Plimpton S. Fast Parallel Algorithms for Short-Range Molecular-Dynamics. J Comput Phys 1995;117(1):1-19.

[30] Kınacı A, Haskins JB, Sevik C, Çağın T. Thermal conductivity of BN-C nanostructures. Phys Rev B 2012;86(11): 115410-1–115410-8.

[31] Dauberosguthorpe P, Roberts VA, Osguthorpe DJ, Wolff J, Genest M, Hagler AT. Structure and Energetics of Ligand-Binding To Proteins - Escherichia-Coli Dihydrofolate Reductase Trimethoprim, a Drug-Receptor System. Proteins 1988;4(1):31-47.

[32] Lee D, Lee B, Park KH, Ryu HJ, Jeon S, Hong SH. Scalable Exfoliation Process for Highly

Soluble Boron Nitride Nanoplatelets by Hydroxide-Assisted Ball Milling. Nano Lett 2015;15(2):1238-1244.

[33] Sudeep PM, Vinod S, Ozden S, Sruthi R, Kukovecz A, Konya Z, et al. Functionalized boron nitride porous solids. Rsc Adv 2015;5(114):93964-93968.

[34] Meng W, Huang Y, Fu Y, Wang Z, Zhi C. Polymer composites of boron nitride nanotubes and nanosheets. J Mater Chem C 2014;2(47):10049-10061.

[35] Chen L, Xiao C, Tang YL, Zhang X, Zheng K, Tian XY. Preparation and properties of boron nitride nanosheets/cellulose nanofiber shear-oriented films with high thermal conductivity. Ceram Int 2019;45(10):12965-12974.

[36] Jitianu A, Britchi A, Badescu V, Deleanu C, Zaharescu M. Influence of the alkoxy group of the Si-alkoxides on the sol-gel process and on the structure of the obtained gels. Rev Roum Chim 2007;52(1-2):93-99.

[37] Pantoja M, Velasco F, Broekema D, Abenojar J, Real JCd. The Influence of pH on the Hydrolysis Process of γ-Methacryloxypropyltrimethoxysilane, Analyzed by FT-IR, and the Silanization of Electrogalvanized Steel. J Adhes Sci Technol 2010;24(6):1131-1143.

[38] Andrade GI, Barbosa-Stancioli EF, Mansur AAP, Vasconcelos WL, Mansur HS. Small-angle X-ray scattering and FTIR characterization of nanostructured poly (vinyl alcohol)/silicate hybrids for immunoassay applications. J Mater Sci 2008;43(2):450-463.

[39] Zhengcai P, Van Ooij WJ, Mark JE. Hydrolysis kinetics and stability of bis(triethoxysilyl)ethane in water-ethanol solution by FTIR spectroscopy. J Adhes Sci Technol 1997;11(1):29-47.

[40] Hamciuc V, Giurgiu D, Marcu M, Butuc E, Ionescu C, Pricop L. Polysulfone-Polydimethylsiloxane Block Copolymers Containing Si-O-C Bonds. J Macromol

Sci Part A-Pure Appl Chem 1998;35(4):563-575.

[41] Guo R, Hu C, Pan F, Wu H, Jiang Z. PVA–GPTMS/TEOS hybrid pervaporation membrane for dehydration of ethylene glycol aqueous solution. J Membr Sci 2006;281(1-2):454-462.

[42] Peng F, Lu L, Sun H, Wang Y, Wu H, Jiang Z. Correlations between free volume characteristics and pervaporation permeability of novel PVA–GPTMS hybrid membranes. J Membr Sci 2006;275(1-2):97-104.

[43] Yang D, Velamakanni A, Bozoklu G, Park S, Stoller M, Piner RD, et al. Chemical analysis of graphene oxide films after heat and chemical treatments by X-ray photoelectron and Micro-Raman spectroscopy. Carbon 2009;47(1):145-152.

[44] Liu R, Xu X, Zhuang X, Cheng B. Solution blowing of chitosan/PVA hydrogel nanofiber mats. Carbohydr Polym 2014;101:1116-1121.

[45] Briggs D, Beamson G. Primary and Secondary Oxygen-Induced C1s Binding-Energy Shifts in X-Ray Photoelectron-Spectroscopy of Polymers. Anal Chem 1992;64(15):1729-1736.

[46] Hassan S, Yusof MS, Embong Z, Maksud MI. Surface adhesion study of La2O3 thin film on Si and glass substrate for micro-flexography printing. AIP Conf Proc 2017;1799: 040006-1–040006-8.

[47] Krishnamoorthy K, Veerapandian M, Yun K, Kim SJ. The chemical and structural analysis of graphene oxide with different degrees of oxidation. Carbon. 2013;53:38-49.

[48] Kariduraganavar MY, Kulkarni SS, Kittur AA. Pervaporation separation of water–acetic acid mixtures through poly(vinyl alcohol)-silicone based hybrid membranes. J Membr Sci 2005;246(1):83-93.

[49] Jiang T, Kuila T, Kim NH, Ku BC, Lee JH. Enhanced mechanical properties of silanized silica nanoparticle attached graphene oxide/epoxy composites. Compos Sci Technol

2013;79:115-125.

[50] Pourhashem S, Vaezi MR, Rashidi A, Bagherzadeh MR. Distinctive roles of silane coupling agents on the corrosion inhibition performance of graphene oxide in epoxy coatings. Prog Org Coat 2017;111:47-56.

[51] Xu YS, Chung DDL. Increasing the thermal conductivity of boron nitride and aluminum nitride particle epoxy-matrix composites by particle surface treatments. Compos Interface. 2000;7(4):243-256.

[52] Guo Y, Ruan K, Shi X, Yang X, Gu J. Factors affecting thermal conductivities of the polymers and polymer composites: A review. Compos Sci Technol 2020; 193: 108134.

[53] Zhang L, Keblinski P, Wang JS, Li B. Interfacial thermal transport in atomic junctions. Phys Rev B 2011;83(6): 064303.

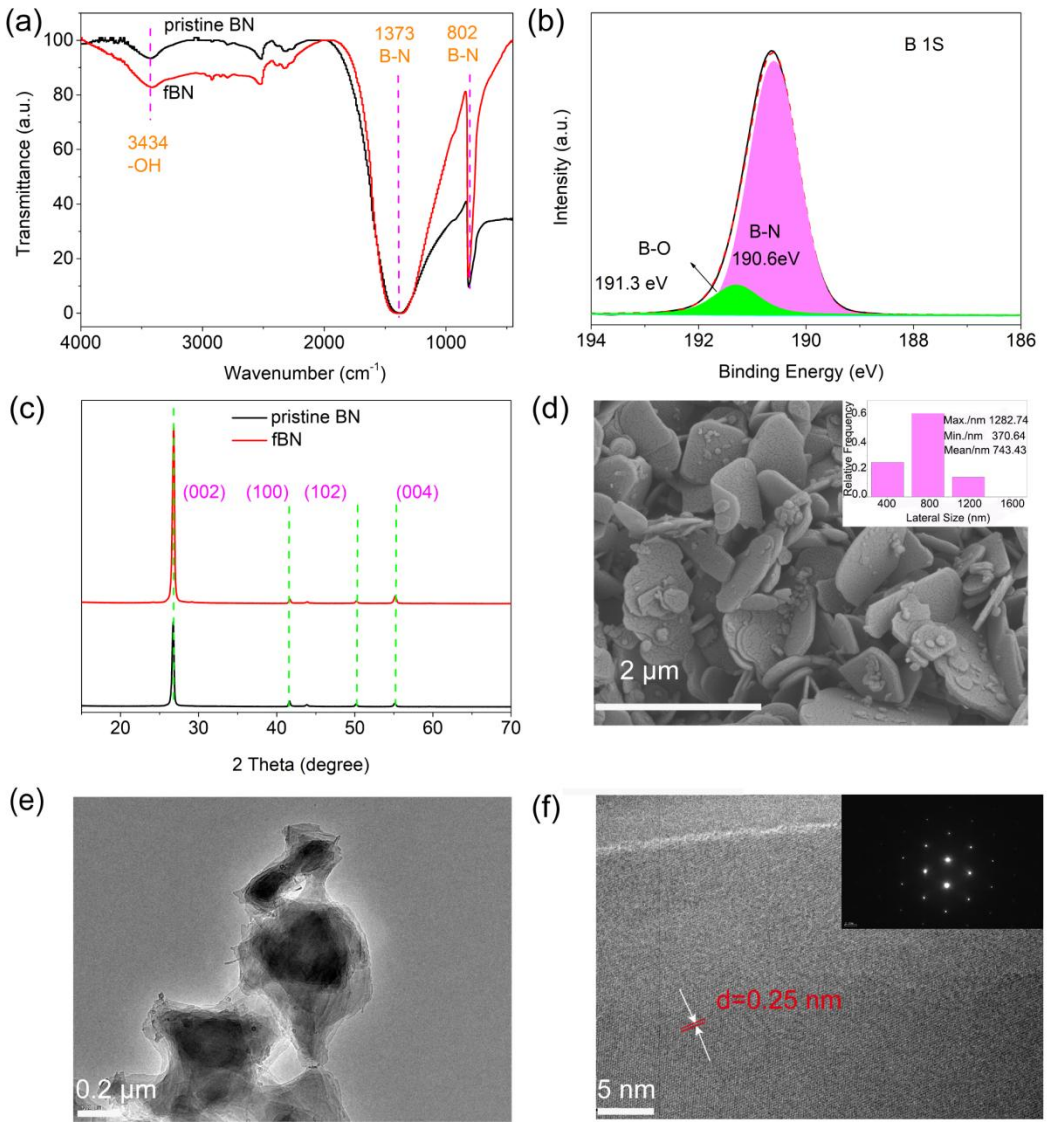

Fig. 1. Characterization of pristine BN and fBN. (a) FT-IR spectra of pristine BN and fBN, (b) high-resolution spectra of B 1s for fBN, (c) XRD patterns of pristine BN and fBN, (d) SEM image of fBN (the inset shows lateral sizes distribution of fBN), (e) TEM morphology of fBN sheets, (f) HR-TEM image of fBN sheets (the inset shows the corresponding Fast Fourier transform image).

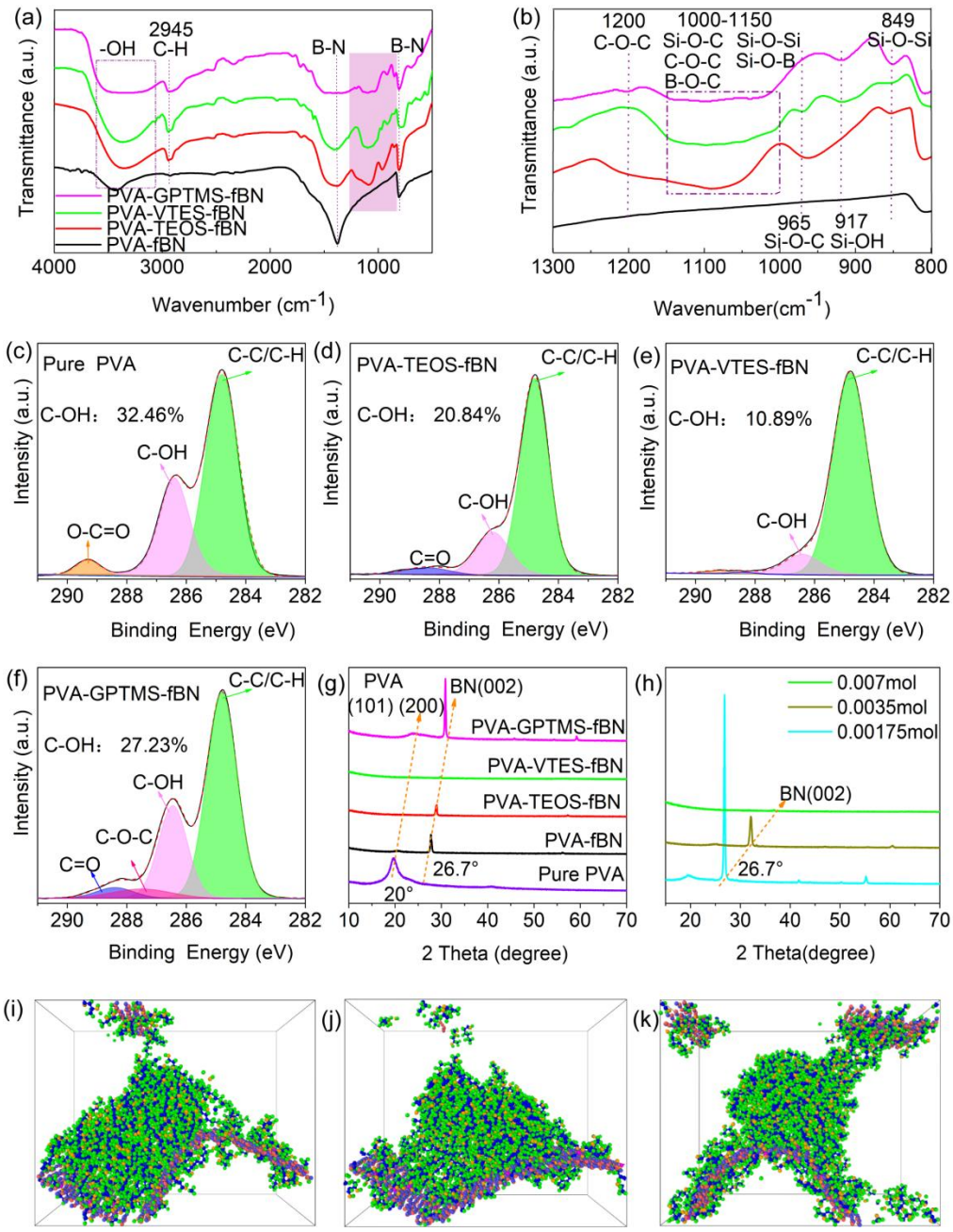

Fig. 2. Characterization of PVA and composites. (a) FT-IR spectra and (b) zoom-in image of composites with 0.007 mol SCAs. High-resolution elemental scans of C1s of (c) pure PVA, (d) PVA-TEOS-fBN, (e) PVA-VTES-fBN and (f) PVA-GPTMS-fBN, (g) XRD pattern of composites with 0.007 mol SCAs, (h) XRD pattern of PVA-VTES-fBN with different VTES

contents. The MD results showing severe deformation of BN layers for, (i) TEOS-, (j) VTES- and (k) GPTMS-bridged system.

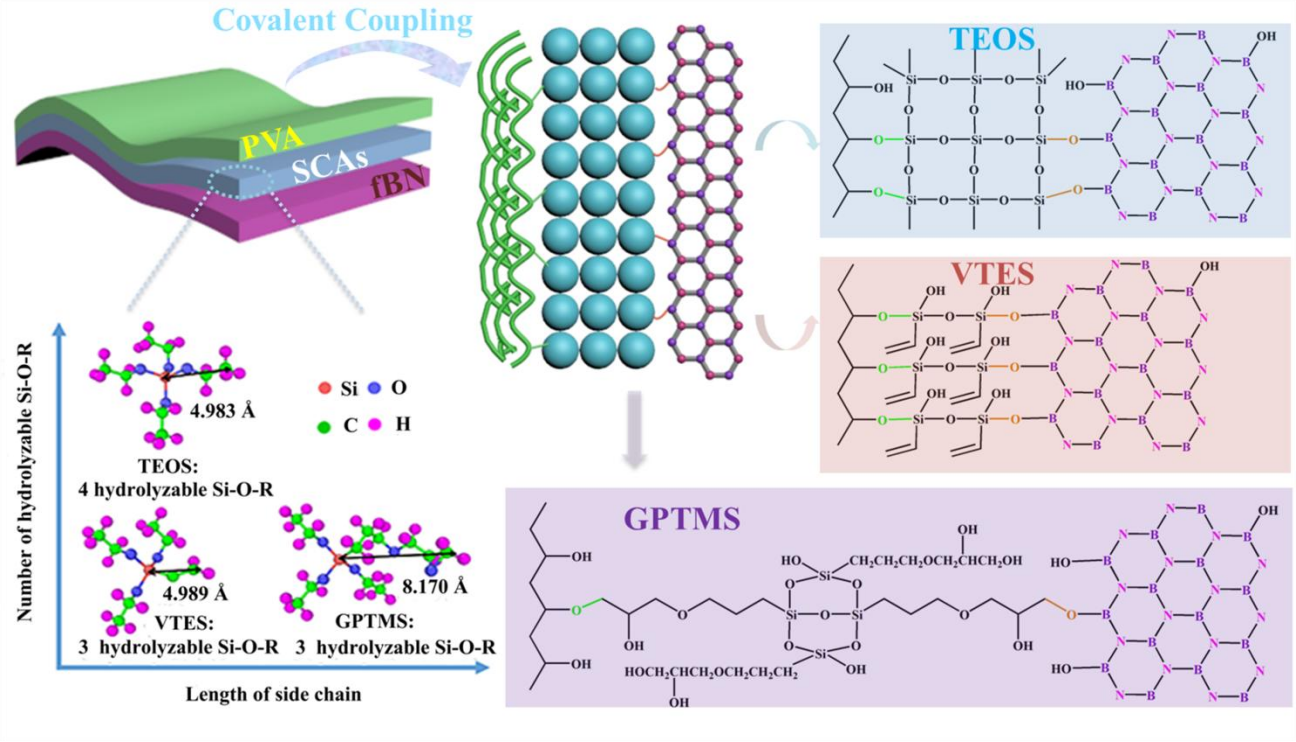

Fig. 3. Schematic of PVA/fBN with different SCAs coupling.

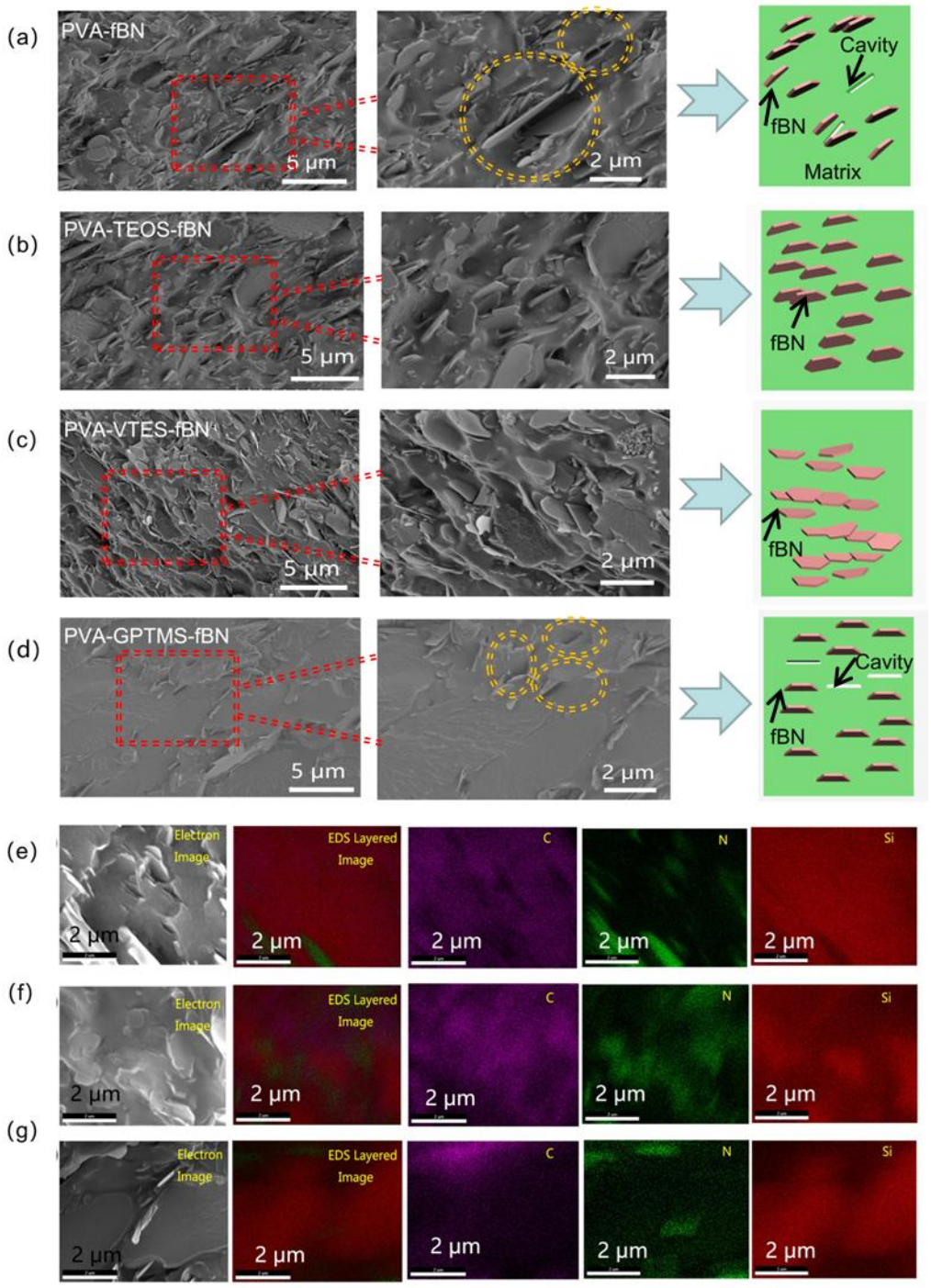

Fig. 4. The cartoon illustration and SEM images of cross-section of PVA-fBN (a), PVA-TEOS-fBN (b), PVA-VTES-fBN (c) and PVA-GPTMS-fBN (d). EDS elemental mapping images of cross-section for PVA-TEOS-fBN (e), PVA-VTES-fBN (f), PVA-GPTMS-fBN (g).

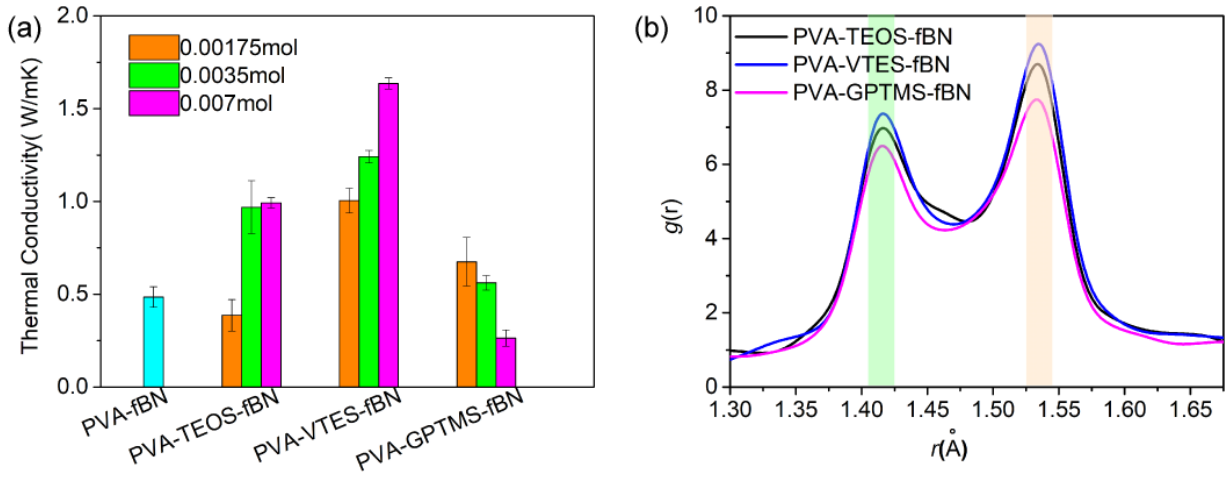

Fig. 5. (a) TC of the composites with different SCAs and various SCAs loadings, (b) radial distribution function (RDF) of the equilibrated PVA-SCAs-fBN system.

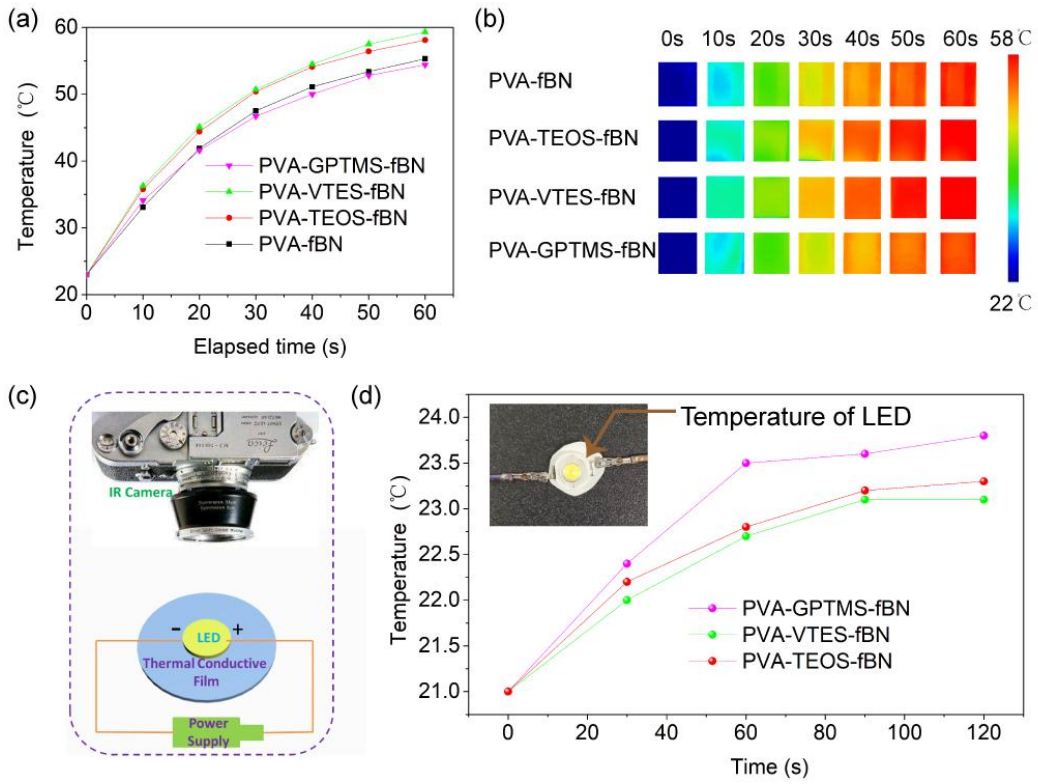

Fig. 6. (a) Temperature evolution with elapsed time and (b) infrared thermal images of the composites with 0.007mol SCAs loading, (c) configuration of LED temperature measurement and (d) working temperature evolution of the LED lamp with composite film substrate (shown in the inset) of 0.007 mol SCAs loading.

Supporting Information of

Covalent coupling regulated thermal conductivity of Poly(vinyl alcohol)/boron nitride composite film based on silane molecular structure

Hua Cheng [‡ a, b, c], *Kai Zhao* [‡d], *Yi Gong* [*a], *Xiao Wang* [e], *Rui Wang* [a, b], *Fengyu Wang* [a], *Rui Hu* [a], *Fangkuo Wang* [c], *Xian Zhang* [a], *Jianying He* [f], *Xingyou Tian* [*a]

[a] Key Laboratory of Photovolatic and Energy Conservation Materials, Institute of Applied Technology, Hefei Institutes of Physical Science, Chinese Academy of Sciences, Hefei 230031, People's Republic of China

[b] University of Science and Technology of China, Hefei 230026, People's Republic of China

[c] Department of Chemistry and Chemical Engineering, Hefei Normal University, Hefei 230061, People's Republic of China

[d] Department of Engineering, Aarhus University, 8000 Aarhus, Denmark

[e] Reservoir Engineering Research Institute, Palo Alto, California 94301, United States

[f] Department of Structural Engineering, Faculty of Engineering, Norwegian University of Science and Technology (NTNU), 7491 Trondheim, Norway

The computational models

The simulations were performed using the open source molecular dynamics (MD) code LAMMPS. Sandwich-like cross-linked interface models as shown in Fig. S1, were built to model the experimental setting-up.

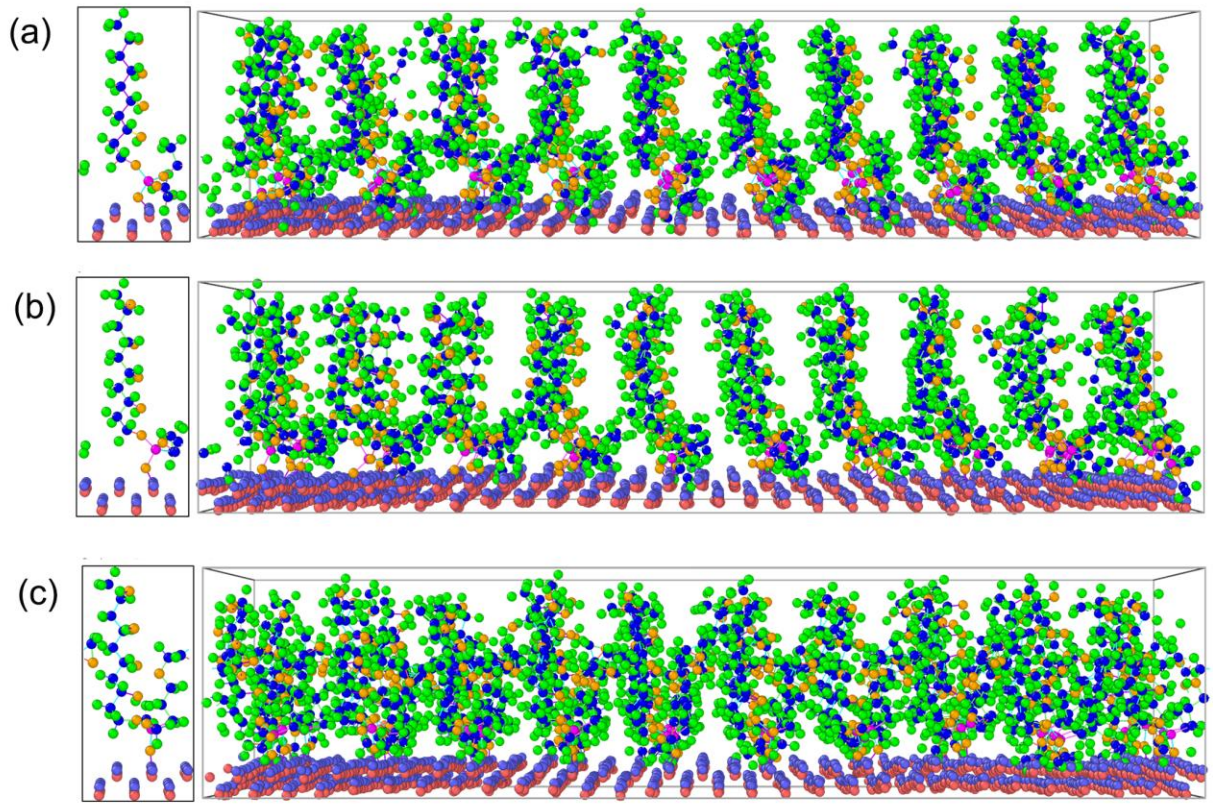

Fig. S1. Sandwich-like configurations used in simulations. The left panel in each sub-figure shows the fundamental structural unit, while the right panel is the 5×2×1 replicated system used for the calculation of TC. (a) PVA-TEOS-fBN, (b) PVA-VTES-fBN, (c) PVA-GPTMS-fBN.

Self-condensation of SCAs

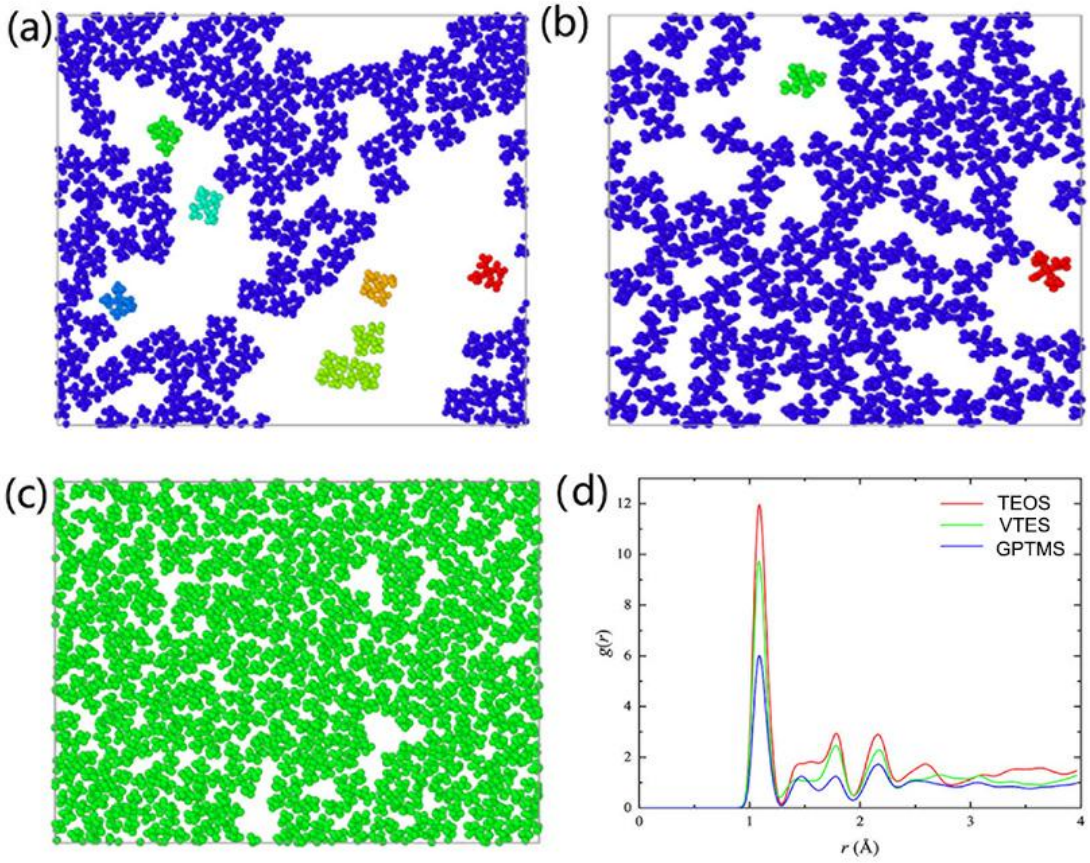

Fig. S2. Self-condensation of (a) TEOS; (b) VTES; (c) GPTMS; (d) The calculation RDF results

Using cluster analysis, Fig. S2 shows that for three different SCAs with the same number of molecules, the TEOS system condensates into 7 clusters, and VTES forms 3 clusters, while the GPTMS molecules distribute homogeneously under room temperature. As shown in Fig. S2(d), the first peak of RDF curves also supports the arguments above.

Mechanical properties of the composites

The typical stress-strain relationship for composites is shown in Fig. S3，and the mechanical properties are summarized in **Table S1**. As expected, the introduction of different kinds of SCAs leads to significant change on mechanical properties. The elongation at break of composite film with GPTMAS and VTES were slightly increased compared to that of PVA/fBN, however, the introduction of TEOS decreased the elongation at break. It is because of that TEOS showed strong tendency of self-condensation after hydrolysis (demonstrated by FT-IR results), forming SiO_2 agglomerates which served as stress concentration sites. Another possible reason may be that the SiO_2 agglomerates restricted the mobility of PVA chains thus resulting the decreasing elongation at break. All the SCAs raised the tensile strength of the composite film. Tensile strength of the composite film with VTES and TEOS increased dramatically due to the abundant chemical bonds between SCAs and PVA/fBN. However, the composite film with GPTMS did not show sharp increment of tensile strength attributing to the weaker bonding effect between and PVA/fBN. It could be found that the mechanical properties of the composites also could be affected by the molecular structure of SCAs via different covalent bonding.

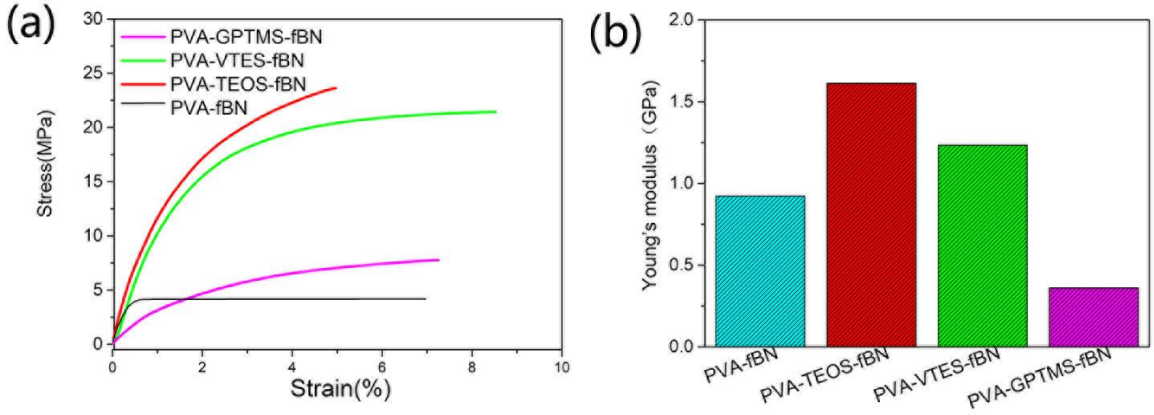

Fig. S3. (a) Typical stress-strain relationship for composites, (b) Young's modulus for the composites

Table S1. Summary of mechanical properties of the composites with different SCAs

Samples	Tensile strength (MPa)	Elongation at break (%)	Young's modulus (GPa)
PVA-fBN	4.18	6.97	0.92
PVA-TEOS-fBN	23.61	4.97	1.61
PVA-VTES-fBN	21.43	8.52	1.23
PVA-GPTMAS-fBN	7.26	7.76	0.36

Chemical reaction of SCA bonding process

Fig. S4, Fig. S5 and Fig. S6 show chemical reactions of hydrolyzed SCAs between PVA and fBN.

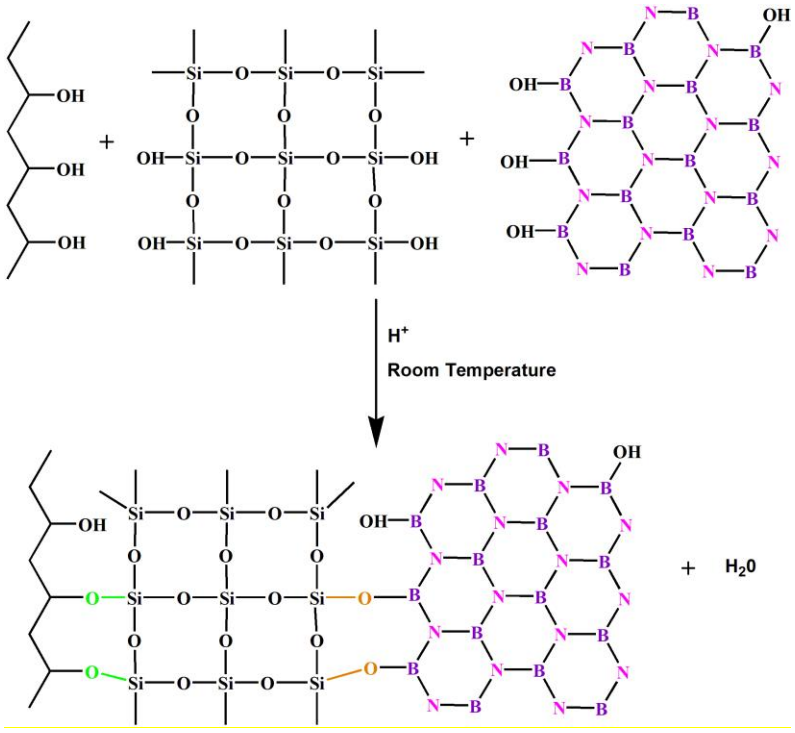

Fig. S4. Chemical reaction of TEOS bonding process between PVA and fBN

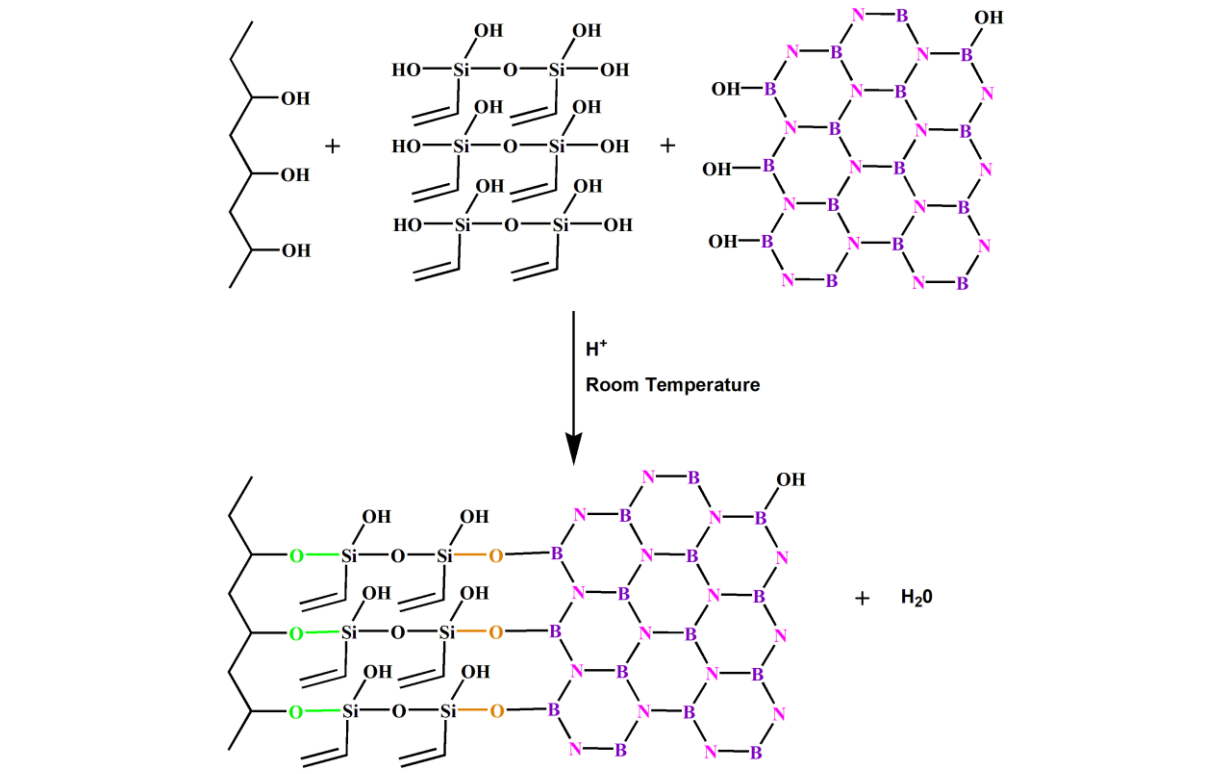

Fig. S5. Chemical reaction of VTES bonding process between PVA and fBN

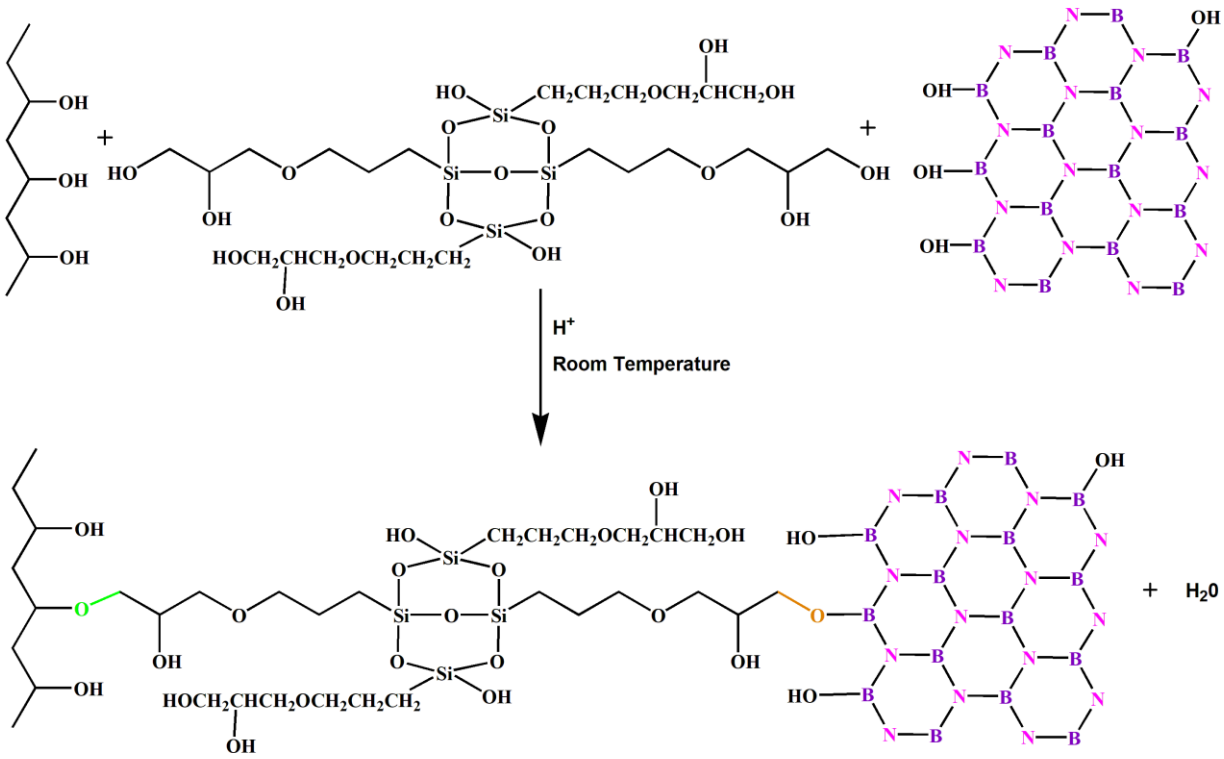

Fig. S6. Chemical reaction of GPTMS bonding process between PVA and fBN

Thermal conductivity Comparison

Creating strong interaction between inorganic fillers and polymer matrix is believed as an effective method to enhance thermal conductivity of composite materials. Different filler functionalization for enhancing interfacial bonding between filler/ polymer have been summarized in Table S2 for TC comparison.

Table S2. Thermal conductivity comparison of polymer composites containing fillers proceeded by different functionalization treatments

Typical Sample	**Functionalization method**	**Filler loading**	**Thermal Conductivity (W/mK)**	**Refs.**
ABS-MFG	Mechanochemical method	15 wt%	0.321	[1]
PA66-GNPs	Plasma treatment	20wt%	3.77	[2]
Epoxy-GNPs	Acid-base treatment	20wt%	1.33	[3]
Epoxy -Graphite	Acid-base treatment	/	0.587	[4]
BNNS-PDA-PVA	Surface coating	70 wt%	24.6	[5]
Epoxy-SiCw	Chemical modifcation	3.91 vol%	0.43	[6]
PI-γ-MPS-BN	Chemical modifcation	40wt%	0.768	[7]
PVA-VTES-fBN	Chemical modifcation	33 wt%	1.636	**This work**

***Abbreviations:**

Acrylonitrile-butadiene-styrene (ABS), multilayer-functionalized graphene (MFG), polyamide 66 (PA66), graphite nanoplatelets (GNPs), boron nitride nanoplatelets (BNNS), polydopamine (PDA), polyvinyl alcohol (PVA), silicon carbide nanowires (SiCw), polyimide (PI), 3-glycidyloxypropyltrimethoxy silane (γ-MPS), boron nitride (BN), vinyl triethoxysilane (VTES), functionalized boron nitride (fBN).

Reference:

[1] Guo Y, Ruan K, Shi X, Yang X, Gu J. Factors affecting thermal conductivities of the polymers and polymer composites: A review. Compos Sci Technol 2020; 193: 108134.

[2] You J, Choi HH, Cho J, Son JG, Park M, Lee SS, et al. Highly thermally conductive and mechanically robust polyamide/graphite nanoplatelet composites via mechanochemical bonding techniques with plasma treatment. Compos Sci Technol 2018;160:245-254.

[3] Xing Z, Sun W, Wang L, Yang Z, Wang S, Liu G. Size-controlled graphite nanoplatelets: thermal conductivity enhancers for epoxy resin. J Mater Sci 2019;54(13):10041-10054.

[4] Wang H, Wang S, Lu W, Li M, Gu Y, Zhang Y, et al. Through-thickness thermal conductivity enhancement of graphite film/epoxy composite via short duration acidizing modification. Appl Surf Sci 2018;442:170-177.

[5] Wang ZG, Chen MZ, Liu YH, Duan HJ, Xu L, Zhou L, et al. Nacre-like composite films with high thermal conductivity, flexibility, and solvent stability for thermal management applications. J Mater Chem C 2019;7(29):9018-9024.

[6] Xiao C, Chen L, Tang Y, Zhang X, Zheng K, Tian X. Enhanced thermal conductivity of silicon carbide nanowires (SiCw)/epoxy resin composite with segregated structure. Compos Pt A-Appl Sci Manuf 2019;116:98-105.

[7] Yang N, Xu C, Hou J, Yao Y, Zhang Q, Grami ME, et al. Preparation and properties of thermally conductive polyimide/boron nitride composites. Rsc Adv 2016;6(22):18279-18287.

Figure(1)

Click here to download high resolution image

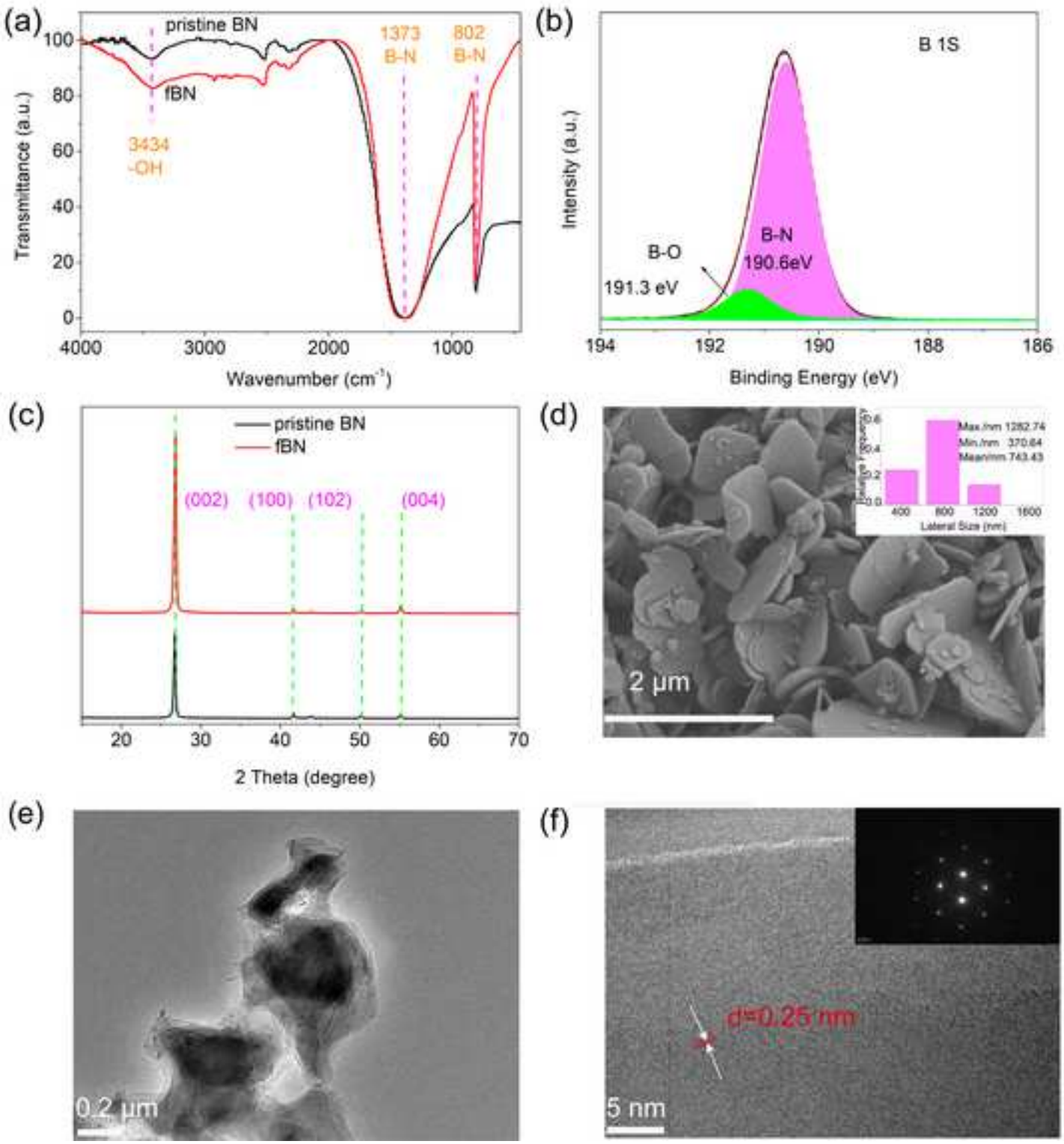

Figure(2)
Click here to download high resolution image

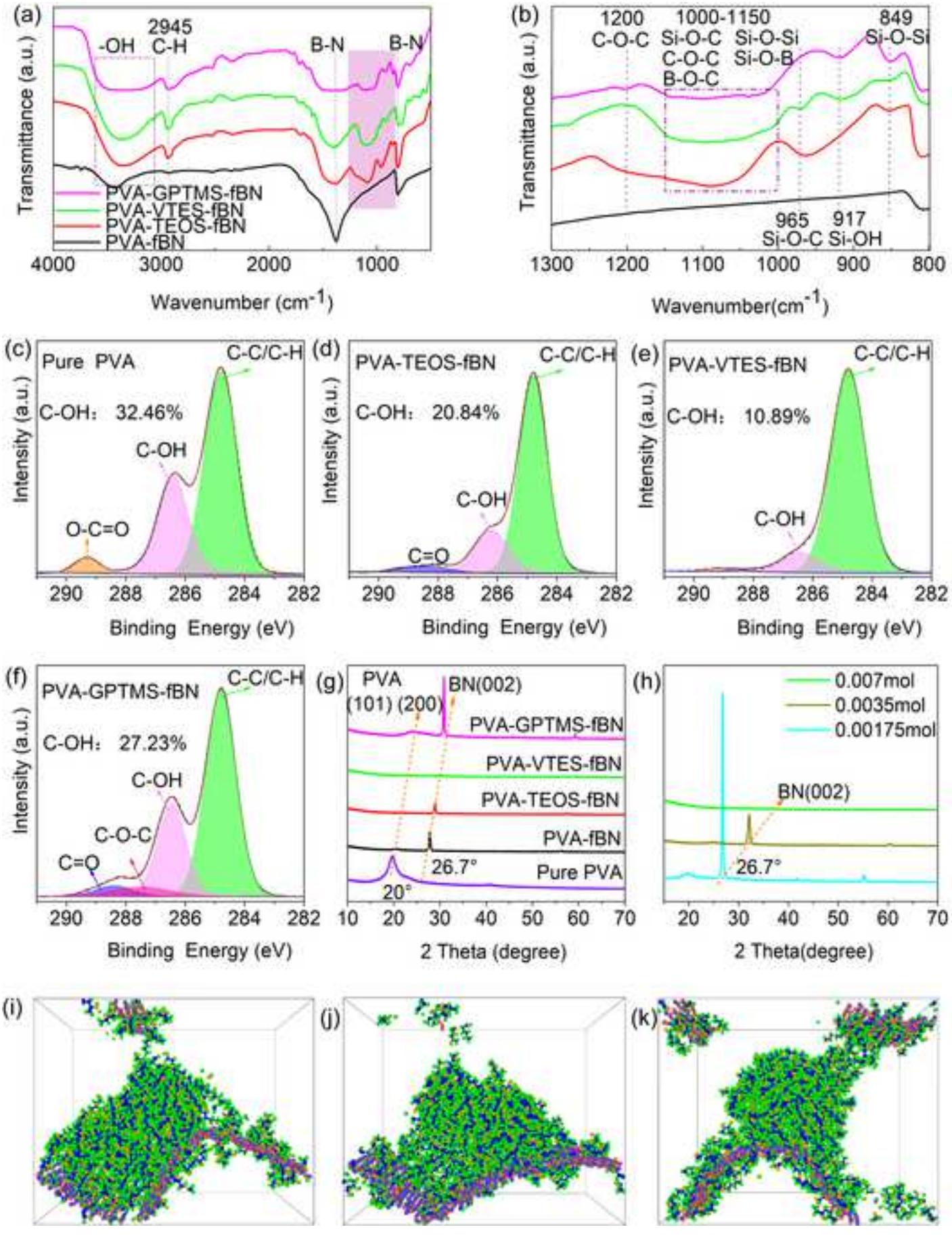

Figure(3)
Click here to download high resolution image

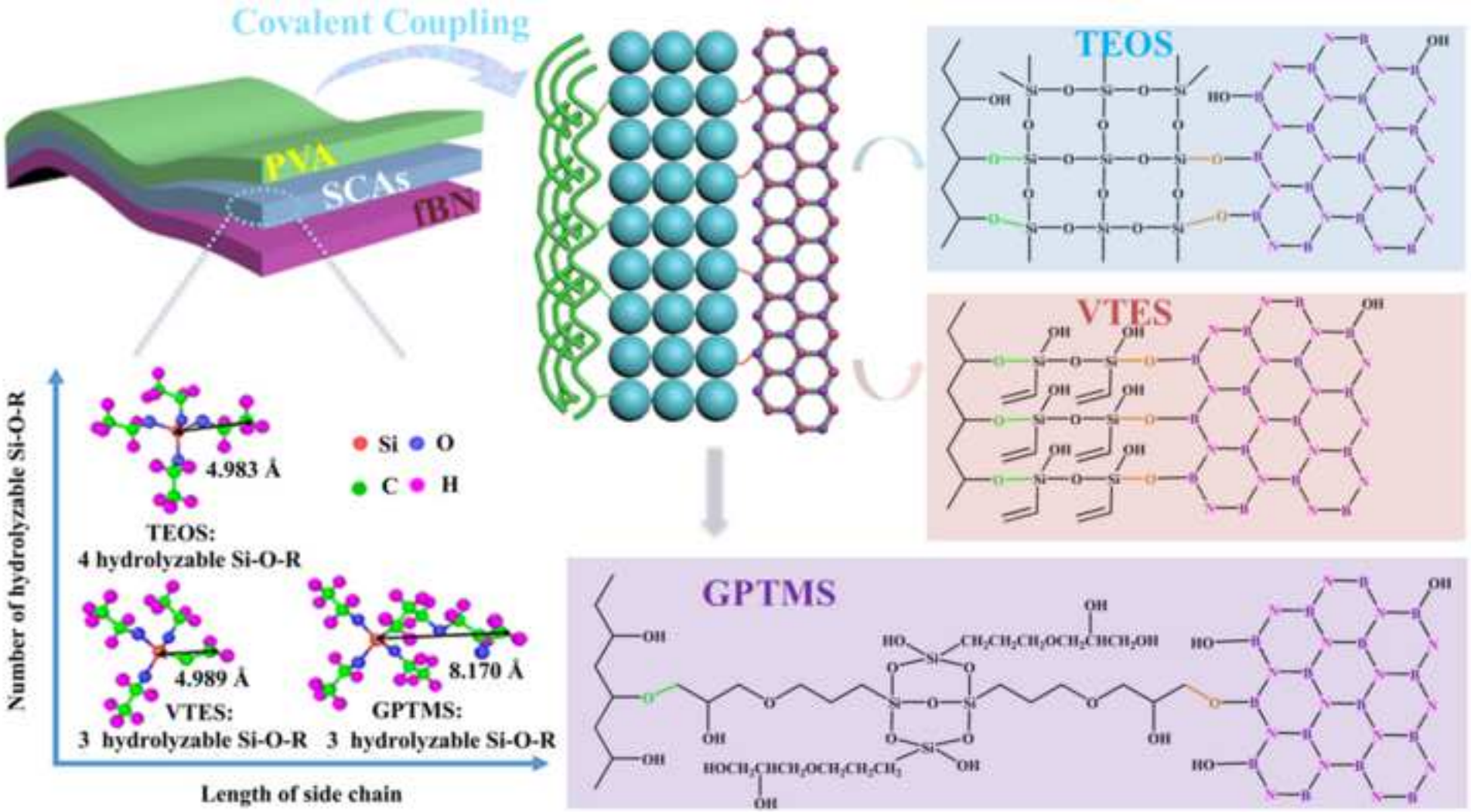

Figure(4)

Click here to download high resolution image

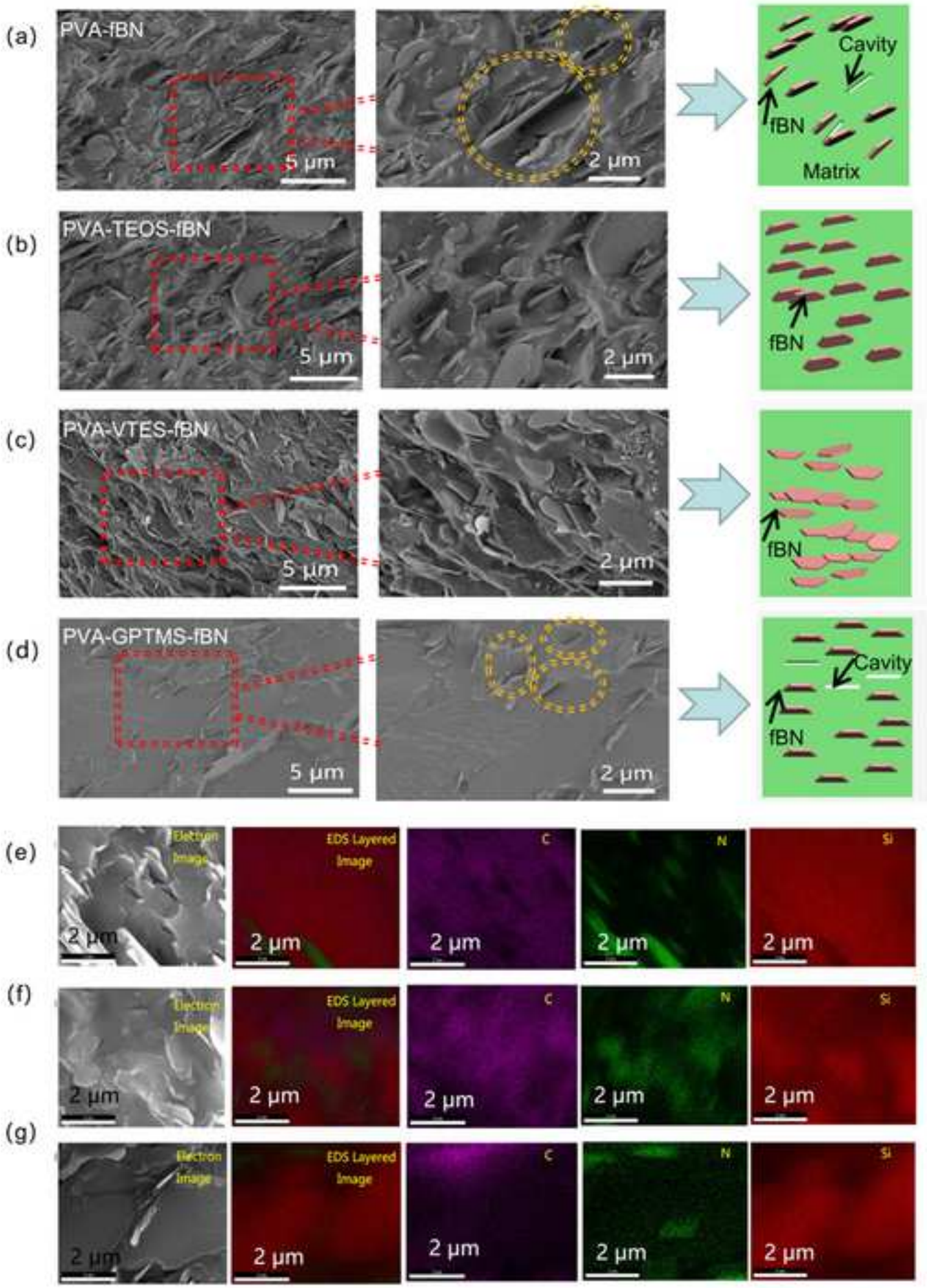

Figure(5)
Click here to download high resolution image

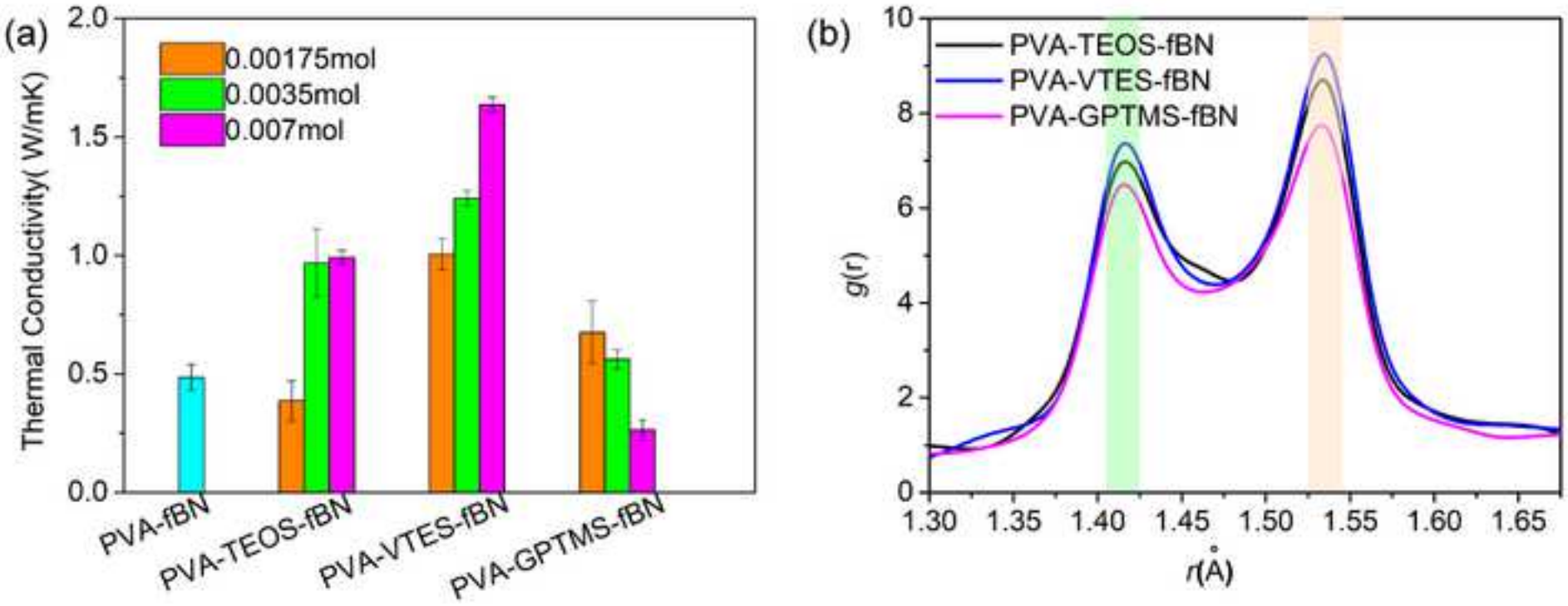

Figure(6)
Click here to download high resolution image

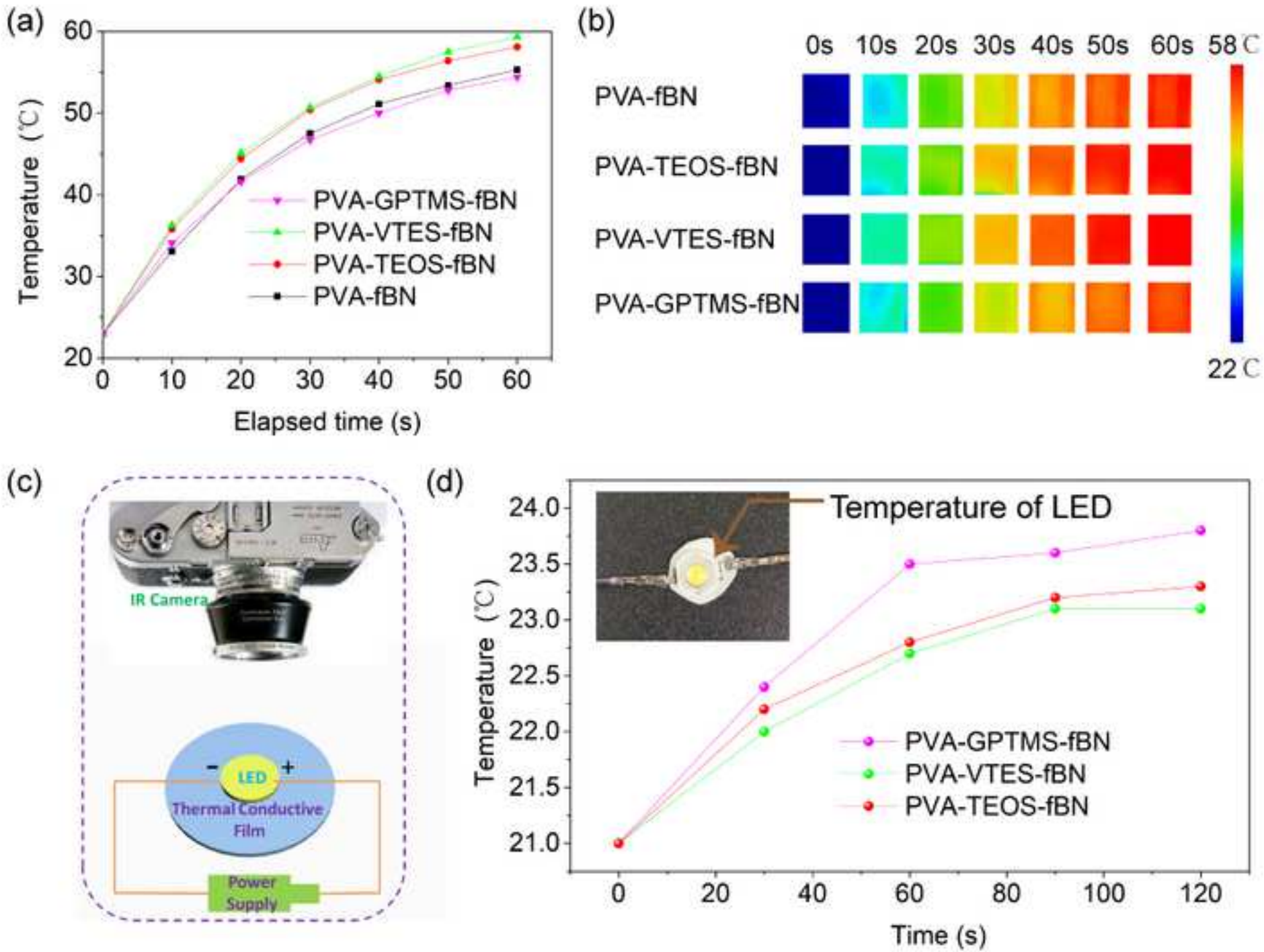

CRediT author statement

Cheng hua: Conceptualization, Methodology , Investigation, Data curation, Writing- original draft. **Zhao kai:** Conceptualization, Methodology, Software Writing - original draft.**Gong Yi:** Conceptualization, Methodology, Writing- review & editing, Supervision, Funding acquisition. **Wang Xiao:** Software. **Rui Wang:** Methodology. **Fengyu Wang:** Methodology, Resources. **Rui Hu:** Data Curation. **Fangkuo Wang:** Writing - review & editing. **Xian Zhang:** Conceptualization, Writing - review & editing, Supervision. **Jianying He:** Writing - review & editing. **Xingyou Tian:** Conceptualization, Writing - review & editing, Funding acquisition.

Cheng hua and **Zhao kai** Contributed equally to this work.

Highlights：

Thermal conductivity (TC) of poly(vinyl alcohol)/boron nitride composite film can be tuned by molecular structure of introduced silane coupling agents (SCAs).

Length of the side chain of SCAs molecules suppresses the TC of composite film.

Number of hydrolyzable Si-O-R of SCAs molecules affects the TC of composite through controlling the self-condensation degree of SCAs.

Owing to the desired molecular structure, VTES improved TC of the composite film to 1.636 W/m·K, best among other investigated SCAs.

***conflict of Interest Statement**

Declaration of interests

☒ The authors declare that they have no known competing financial interests or personal relationships that could have appeared to influence the work reported in this paper.

☐The authors declare the following financial interests/personal relationships which may be considered as potential competing interests: